Available online at www.sciencedirect.com
ScienceDirect
ELSEVIER
Ocean Engineering 33 (2006) 2067–2082
OCEAN ENGINEERING
www.elsevier.com/locate/oceaneng

Bragg reflection of sinusoidal waves due to trapezoidal submerged breakwaters

Chan-Hoo Jeon[a], Yong-Sik Cho[b,*]

[a] *Civil Engineering Division, Hyundai Institute of Construction Technology, Mabuk-ri 102-4, Yongin-si, Gyounggi-do 449-716, Republic of Korea*

[b] *Department of Civil Engineering, Hanyang University, 17 Haengdang-dong, Seongdong-gu, Seoul 133-791, Republic of Korea*

Received 19 January 2005; accepted 13 July 2005
Available online 28 February 2006

Abstract

Numerical and laboratory experiments are performed to investigate characteristics of the Bragg reflection due to multi-arrayed trapezoidal submerged breakwaters. The numerical model is based on the Reynolds averaged Navier–Stokes equations with the VOF method and the k–ε turbulence closure model. As expected, the reflection coefficients increase as the array of submerged breakwaters increases in both laboratory measurements and numerical results. The resonant periods provide similar relative wave numbers regardless of the permeability and the number of arrays. The reflection coefficients due to porous breakwaters are smaller than those due to non-porous breakwaters. The velocity contours for two and three arrays are also described.

Keywords: Bragg reflection; Trapezoidal submerged breakwater; Sinusoidal wave; Navier–Stokes equations

*Corresponding author. Fax: 82 2 2293 9977.
E-mail address: ysc59@hanyang.ac.kr (Y.-S. Cho).

doi:10.1016/j.oceaneng.2005.07.013

Notations

ρ	density of a fluid
g_i	ith component of the gravitational acceleration
μ	molecular viscosity
W_b	bottom width of the trapezoidal submerged breakwater
W_t	top width of the trapezoidal submerged breakwater
h_s	height of the trapezoidal submerged breakwater
h	water depth
d	space between two breakwaters
m	the number of submerged breakwaters
f_p	peak frequency
Δl	separation distance
$f_{\min}$	lower limit of the effective frequency range
$f_{\max}$	upper limit of the effective frequency range
$\lambda_{\min}$	wavelength corresponding to $f_{\min}$
$\lambda_{\max}$	wavelength corresponding to $f_{\max}$

1. Introduction

Propagating from deep water into shallow water, water waves may experience various transformations such as diffraction, refraction, reflection and shoaling due to change of bottom topographies or interferences with structures. Water waves may play significant roles in change of coastal climate. There are many efforts to minimize unwanted coastal erosion and deposit by using artificial structures such as groins and submerged breakwaters.

Recently, submerged breakwaters are widely used because of several advantages over other structures. Firstly, they reflect a significant amount of the incident wave energy. Secondly, because they are constructed under water, it is possible to improve the sea environment and preserve the ecosystem. Thirdly, they improve the harbor tranquility. And if the concept of the Bragg reflection, which occurs when the wave number of the incident wave is approximately equal to twice that of the corrugated bottom topography, is adapted to the design of submerged breakwaters, their effects will become much more significant.

Cooker et al. (1990) studied the interaction between a solitary wave and a semicircular submerged cylinder with numerical analysis and laboratory experiments. Laboratory and the numerical analyses of waves past a submerged porous step were conducted by Losada et al. (1997). Mase et al. (2000) carried out laboratory experiments on Bragg scattering of waves due to submerged breakwaters and measured reflection coefficients. Cho et al. (2001) recommended a trapezoidal shape for submerged breakwaters after comparing the reflecting capability and construction feasibility of various types of submerged breakwaters by using the eigenfunction expansion method (hereinafter EFEM). Hwung et al. (2002) performed a laboratory study on wave transformation over a submerged breakwater.

In this study, characteristics of the Bragg reflection due to the trapezoidal submerged, both non-porous and porous, breakwaters are investigated by numerical methods and laboratory experiments for incident sinusoidal waves. The numerical model employs the Reynolds averaged Navier–Stokes equations (hereinafter RANS) as the governing equations and the volume of fluid (VOF) method as the numerical scheme. And, in the case of the non-porous structures, the results of the EFEM model are also described.

2. Governing equations

2.1. RANS equations

For a turbulent flow, the velocity field is decomposed into the mean velocity $\langle u_i \rangle$ and turbulent velocity u_i' and also the pressure field is separated into the mean pressure $\langle P \rangle$ and turbulent pressure P'. Thus, the velocity and the pressure fields can be described as

$$u_i = \langle u_i \rangle + u_i', \quad P = \langle P \rangle + P', \tag{1}$$

where $i = 1, 2, 3$ for a three-dimensional flow. If the flow is assumed to be incompressible, the mean flow is governed by the Reynolds equations given by (Lin and Liu, 1998)

$$\frac{\partial \langle u_i \rangle}{\partial x_i} = 0, \tag{2}$$

$$\frac{\partial \langle u_i \rangle}{\partial t} + \langle u_j \rangle \frac{\partial \langle u_i \rangle}{\partial x_j} = -\frac{1}{\rho}\frac{\partial \langle P \rangle}{\partial x_i} + g_i + \frac{1}{\rho}\frac{\partial \langle \tau_{ij} \rangle}{\partial x_j} - \frac{\partial \langle u_i' u_j' \rangle}{\partial x_j}, \tag{3}$$

in which ρ is the density of a fluid and g_i is the ith component of the gravitational acceleration. And, $\langle \tau_{ij} \rangle$ is the viscous stress tensor of the mean flow and can be expressed as $2\mu\langle \sigma_{ij} \rangle$ with the molecular viscosity μ and the rate of strain tensor of the mean flow $\langle \sigma_{ij} \rangle$, where $\langle \sigma_{ij} \rangle$ is described as (Liu and Lin, 1997)

$$\langle \sigma_{ij} \rangle = \frac{1}{2}\left(\frac{\partial \langle u_i \rangle}{\partial x_j} + \frac{\partial \langle u_j \rangle}{\partial x_i}\right). \tag{4}$$

2.2. k–ε model

The governing equations for k and ε can be derived from the Navier–Stokes equations given by (Lin and Liu, 1998)

$$\frac{\partial k}{\partial t} + \langle u_j \rangle \frac{\partial k}{\partial x_j} = \frac{\partial}{\partial x_j}\left[\left(\frac{v_t}{\sigma_k} + v\right)\frac{\partial k}{\partial x_j}\right] - \langle u_i' u_j' \rangle \frac{\partial \langle u_i \rangle}{\partial x_j} - \varepsilon, \tag{5}$$

$$\frac{\partial \varepsilon}{\partial t} + \langle u_j \rangle \frac{\partial \varepsilon}{\partial x_j} = \frac{\partial}{\partial x_j}\left[\left(\frac{v_t}{\sigma_\varepsilon} + v\right)\frac{\partial \varepsilon}{\partial x_j}\right] + C_{1\varepsilon}\frac{\varepsilon}{k} v_t \left(\frac{\partial \langle u_i \rangle}{\partial x_j} + \frac{\partial \langle u_j \rangle}{\partial x_i}\right)\frac{\partial \langle u_i \rangle}{\partial x_j} - C_{2\varepsilon}\frac{\varepsilon^2}{k}, \tag{6}$$

where σ_k, σ_ε, $C_{1\varepsilon}$ and $C_{2\varepsilon}$ are empirical coefficients.

2.3. Porous media

Because the structure of porous materials is complex, it is infeasible to solve the Navier–Stokes equations directly in porous pores. Conventionally, the Navier–Stokes equations are averaged over a length scale l_p. Thus, a fluid variable is decomposed into a spatially averaged and a spatially fluctuated quantities. That is, u_i is described as $(\bar{u}_i + u_i'')/n$ and P_0 is expressed as $\bar{P}_0 + P_0''$ with n being the effective porosity of a porous medium. The spatially averaged Navier–Stokes equations are represented by (Liu et al., 1999)

$$\frac{\partial \bar{u}_i}{\partial x_i} = 0, \tag{7}$$

$$\frac{1 + c_A}{n}\frac{\partial \bar{u}_i}{\partial t} + \frac{\bar{u}_j}{n^2}\frac{\partial \bar{u}_i}{\partial x_j} = -\frac{1}{\rho}\frac{\partial \bar{P}_0}{\partial x_i} + \frac{v}{n}\frac{\partial^2 \bar{u}_i}{\partial x_j \partial x_j} - \frac{1}{n^2}\frac{\partial \bar{u}_i'' \bar{u}_j''}{\partial x_j}. \tag{8}$$

3. VOF method

The VOF method is a means to identify different types of computational cells and thus can be used efficiently to track the free surface motion. The density change equation is used to track the free surface given as (Lin, 1998)

$$\frac{\partial \rho}{\partial t} + u_i \frac{\partial \rho}{\partial x_i} = 0. \tag{9}$$

By letting $\rho(x, y, t) = F(x, y, t)\rho_f$, and substituting this definition and Eq. (2) into Eq. (9), we can obtain the transport equation for $F(x, y, t)$ as

$$\frac{\partial F}{\partial t} + \frac{\partial}{\partial x}(uF) + \frac{\partial}{\partial y}(vF) = 0. \tag{10}$$

In this study, the Hirt and Nichols' (1981) algorithm in which the free surface is reconstructed either horizontally or vertically in each free surface cell based on the F values at the nth time step is used.

4. Laboratory experiments

4.1. Experimental facilities

Laboratory experiments have been conducted in a wave tank of 0.6 m wide, 1.1 m high and 32.5 m long. The wave tank is equipped with an electric servo piston-type

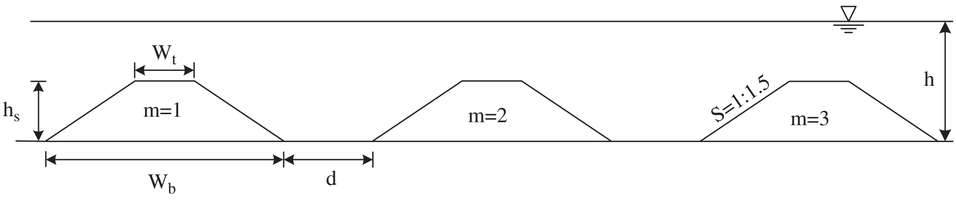

Fig. 1. Schematic plot of trapezoidal submerged breakwaters.

wave-maker that is able to change the wave period and height successively. And the feed back control of wave re-reflection wave gages located in front of the paddle is possible. Manifold porous structures are set up on both sides of the wave flume to absorb waves.

As shown in Fig. 1, the bottom width (W_b) of a trapezoidal submerged breakwater is 1.6 m, the top width (W_t) is 0.4 m, the height (h_s) is 0.4 m, the slope is 1:1.5, the water depth (h) is 0.8 m and the space (d) between two adjacent breakwaters is 2.0 m. In the case of a porous medium, the breakwater is made of model tetrapods (T.T.P.) with the porosity of 0.5. The effective diameter of the tetrapod is estimated as 0.076 m. In the figure, m means the array number of submerged breakwaters.

4.2. Measurements of reflection coefficients

The zero-upcrossing method is employed to analyze water waves generated by the wave paddle in laboratory. The wave flume used in laboratory has been set up as the system that generates an equal wave before and after installation of structures by absorbing re-reflected waves and adjusting the wave signals.

The separation of incident and reflected waves is carried out by Goda and Suzuki's (1976) method based on data obtained from two wave gages installed arbitrarily in front of structures. The frequency band to resolve is $0.6f_p$–$0.3f_p$ with f_p being the peak frequency, and the separation distance Δl can be calculated as

$$\text{Upper limit } (f_{\max}):\ \Delta l/\lambda_{\min} = 0.45, \tag{11}$$

$$\text{Lower limit } (f_{\min}):\ \Delta l/\lambda_{\max} = 0.05, \tag{12}$$

where $\lambda_{\min}$ and $\lambda_{\max}$ are the wavelengths corresponding to the upper limit $f_{\max}$ and lower limit $f_{\min}$ of the effective frequency range, respectively.

5. Numerical analysis

5.1. Mesh generation for a computational domain

The size of the computational domain is $55.0\,\text{m} \times 1.0\,\text{m}$. The uniform grid system of $\Delta x = 0.1$ m is used in the x-direction and two kinds of grids are used in the

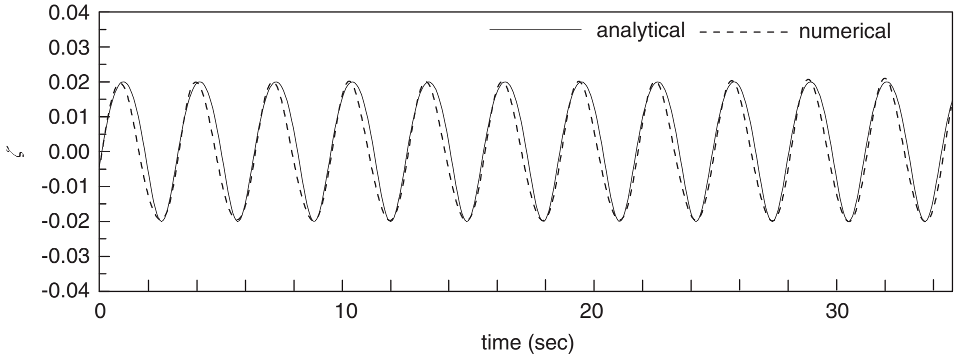

Fig. 2. Comparison of the analytical and the numerical solutions.

y-direction to save the computational time. The grid with $\Delta y = 0.01$ m is used in the region between the bottom and the point where trapezoidal submerged breakwaters are installed, and the section where the free surface is included, while the grid of $\Delta y = 0.02$ m is adapted in the rest of the region. The water depth is 0.8 m and the incident wave height is 0.04 m.

Submerged breakwaters are located at the distance of twice as far as the incident wavelength from the wave paddle. The internal wave-maker is installed at 2.0–5.0 m from the origin point that generates the target wave very closely. In this study, the incident wave periods are 1.1426–3.7333 s and the relative wave numbers (kh) are 0.5–2.5.

5.2. Internal wave generation

The internal wave-maker should be located between the half of the water depth and the trough. Thus, in this study, the internal wave-maker is located at 0.40–0.78 m because the water depth is 0.8 m and the wave height is 0.04 m.

In Fig. 2, the calculated time history of the incident wave profile is compared with the analytical solution. The incident wave is a sinusoidal wave and the wave height is 0.04 m. As shown in the figure, the numerical results agree well with the analytical solutions.

6. Results and discussion

6.1. Reflection coefficients

Figs. 3–7 show reflection coefficients of water waves over a train of submerged non-porous and porous breakwaters for different arrays. The results of the VOF and the EFEM models are compared with experimental measurements for non-porous breakwaters, whereas the results of VOF model are compared with porous breakwaters.

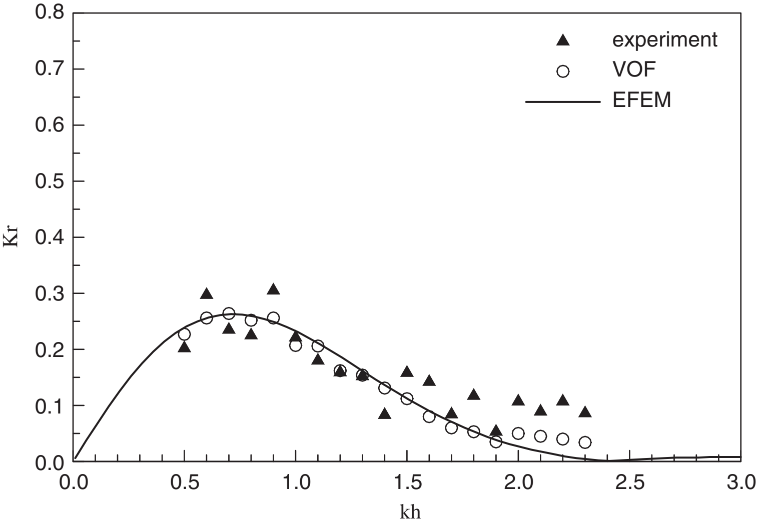

Fig. 3. Reflection coefficients due to non-porous breakwaters ($m = 1$).

Fig. 3 shows reflection coefficients of trapezoidal submerged non-porous breakwaters installed in one array with an interval of 2.0 m. As shown in the figure, the numerical results of VOF model agree comparatively well with those of EFEM model and experimental measurements. However, a slight discrepancy is observed for $kh > 2.0$. The reflection coefficient takes the maximum value of 0.25 when the relative wave number, kh, is approximately 0.7 and the only one peak occurs.

Fig. 4 represents the case of trapezoidal submerged non-porous breakwaters installed in two arrays with an interval of 2.0 m. As shown in the figure, the numerical results of the VOF model agree fairly well with experimental measurements and those values calculated by the EFEM model. When the period of the incident wave is short ($kh > 2.0$), the results of the EFEM model show slight discrepancies with those of the laboratory experiments, while the results obtained from the VOF model agree very well with the measurements. These discrepancies are generated because the EFEM is based on the linear wave theory, while the VOF model considers the non-linearity. The first resonance period is generated at kh of approximately 0.6 and the second at kh of about 1.3, and the maximum reflection coefficient is about 0.5.

Reflection coefficients of the submerged porous breakwaters made of T.T.P. in two arrays with an interval of 2.0 m are shown in Fig. 5. Comparisons between the numerical results of the VOF model and experimental measurements are made in the figure. By comparing with reflection coefficients of submerged non-porous breakwaters, those of porous breakwaters show similar resonance periods but magnitudes are smaller. This phenomenon is caused by the energy dissipation of the incident

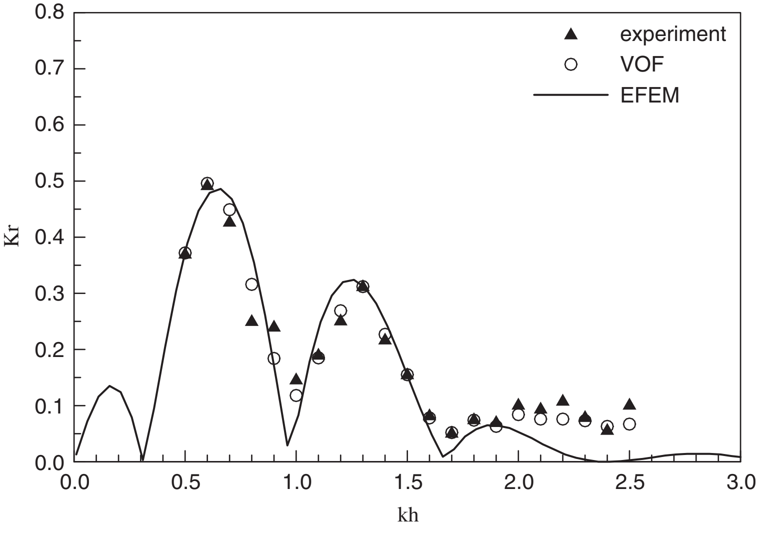

Fig. 4. Reflection coefficients due to non-porous breakwaters ($m = 2$).

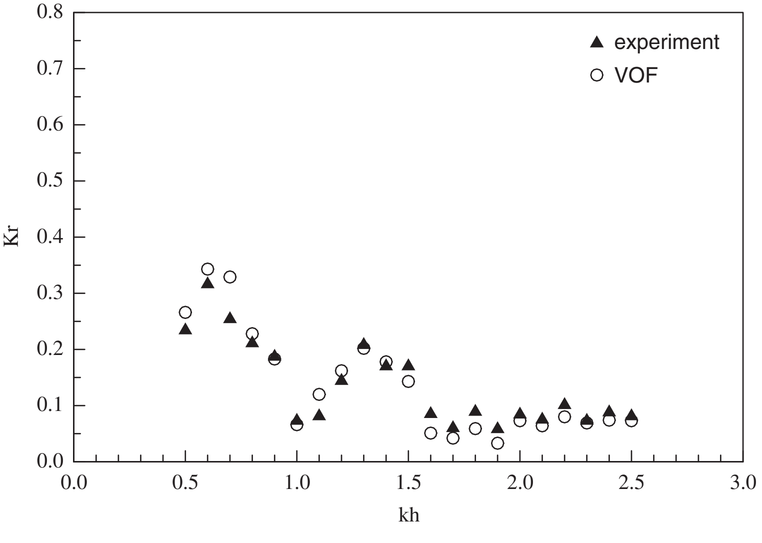

Fig. 5. Reflection coefficients due to porous breakwaters ($m = 2$).

wave due to porous structures. It is noted that the reflection coefficient due to porous structures appears about 66% of that due to non-porous structures for the first resonance period.

Fig. 6 shows distribution of reflection coefficients of submerged non-porous breakwaters consisted of three arrays with an interval of 2.0 m. It is obvious that

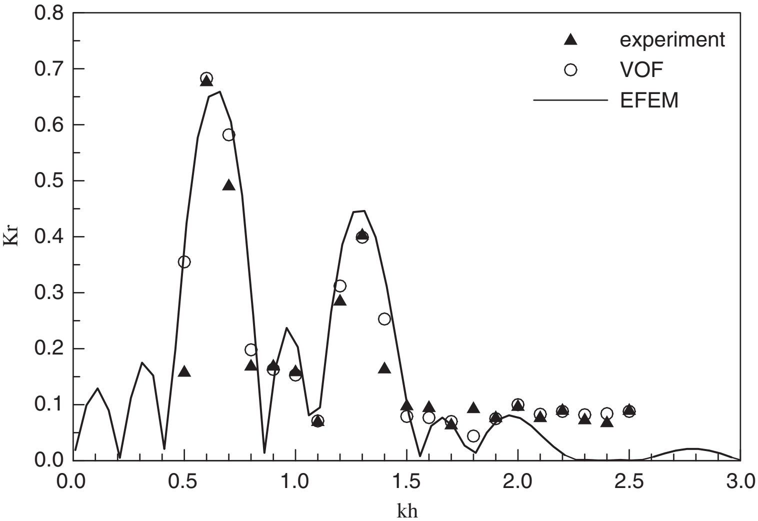

Fig. 6. Reflection coefficients due to non-porous breakwaters ($m = 3$).

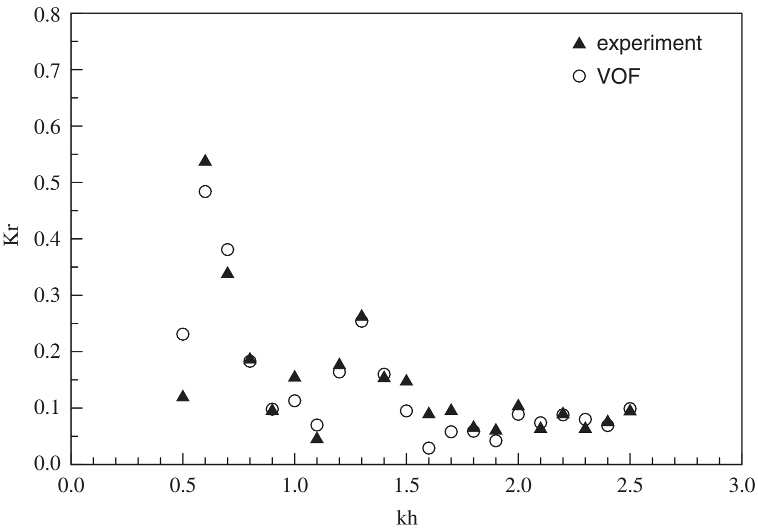

Fig. 7. Reflection coefficients due to porous breakwaters ($m = 3$).

there are excellent agreements between the numerical results obtained from the VOF model and experimental measurements. As in the case of two arrayed submerged non-porous breakwaters, the EFEM results show a good agreement with experimental measurements for $kh = 0.5$–2.0, while slight discrepancies are observed for $kh > 2.0$. It is clear that the maximum value of the reflection coefficients appears for $kh \approx 0.7$ and the second resonance period for $kh \approx 1.3$. The reflection coefficient of the first resonance period is 0.67 in the experimental measurements and 0.68 in the numerical results.

Fig. 7 displays reflection coefficients of submerged porous breakwaters consisted of T.T.P. installed three arrays at an interval of 2.0 m. The numerical results of the VOF model and the laboratory data are very agreeable. By comparing the results of the porous breakwaters with those of the non-porous breakwaters, we can observe that the reflection coefficients due to porous breakwaters are smaller than those due to non-porous breakwaters for relatively long waves, while they show very slight discrepancies for relatively short waves. These differences may be caused by the experimental condition which becomes the deep water when the period of the incident wave is short. Thus, the effects of the submergence are not significant.

As shown in Figs. 3–7, the numerical results of the VOF model agree very well with experimental measurements for the non-porous structures, while there are slight discrepancies for the porous structures. This is because of the following reasons: (1) the inaccuracy in modeling flows in the submerged porous breakwaters could affect the free surface simulation nearby; and (2) in the VOF model, the partial cell treatment, which enables to represent inclined boundaries, is disabled when submerged porous breakwaters are considered, so the sawtooth shape of the horizontal and vertical boundaries is used.

Figs. 8 and 9 show the characteristics of the reflection coefficients for the laboratory experiments and the VOF model, respectively. In both laboratory experiments and the numerical analyses, the values of kh where the resonance

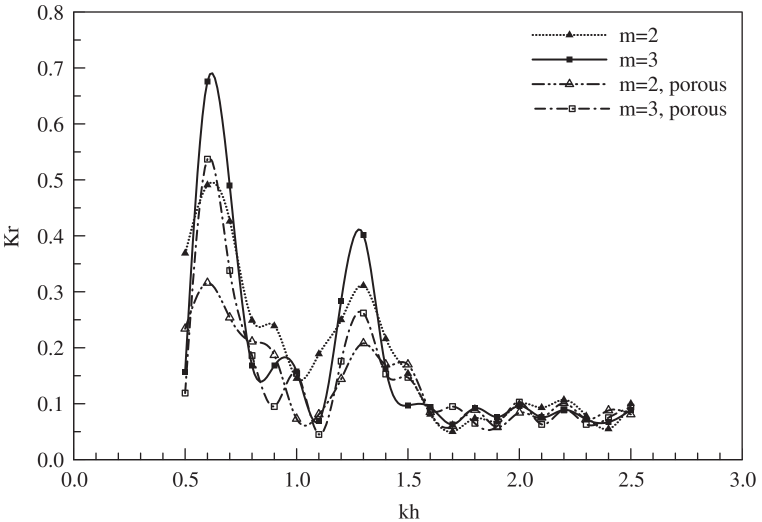

Fig. 8. Comparison of the experimental data according to the characteristics of submerged breakwaters.

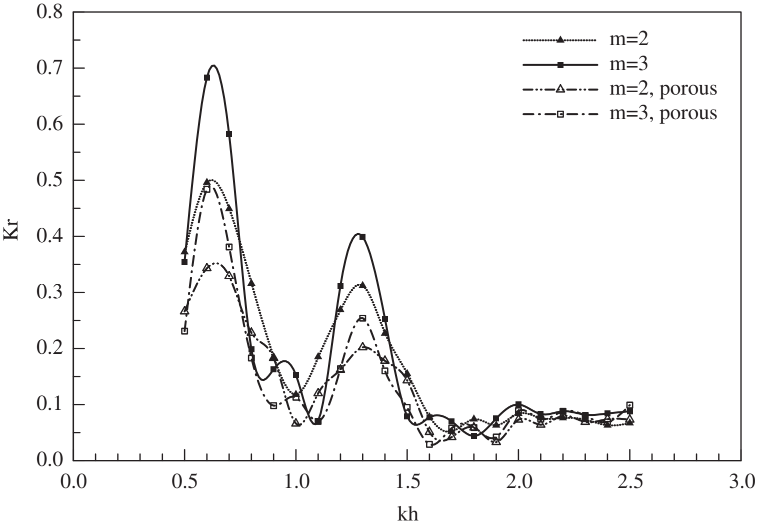

Fig. 9. Comparison of the numerical results (VOF model) according to the characteristics of submerged breakwaters.

appears are very similar regardless of the number of arrays and whether porous or non-porous. On the whole, the first resonance is generated for $kh = 0.6$–0.7 and the second for $kh = 1.3$–1.4. The reflection coefficients increase in proportion as the number of structures increases. The values due to non-porous breakwaters are larger than those due to porous breakwaters. But, whether the structures are porous or non-porous does not influence the reflection coefficients for short waves. This means that short waves are not distorted by the change of bottom topography.

6.2. Velocity contour

Figs. 10–13 show velocity contours around submerged breakwaters. The incident wave height is 0.04 m and the period is 3.1614 s. The snapshots of velocity contours are taken at times of 32.0, 40.0 and 48.0 s after the generation of waves.

Fig. 10 displays the case of submerged non-porous breakwaters in two arrays. It is noted that the magnitude of velocity increases at the upper side of the first arrayed breakwater and decreases at the back side of the structures. And, Fig. 11 represents the case of submerged porous breakwaters of two arrays. The flow exists in porous structures and the velocities at the upper and back side of breakwaters are different for the non-porous case. The velocities at the upper side of the first arrayed breakwater are smaller than those of the non-porous.

Fig. 12 describes the case of submerged non-porous breakwaters of three arrays. Compared with the case of two arrays, the velocities in front of breakwaters are larger and those at the back side are smaller. Similarly with the two arrayed case, the flow is fastest at the upper side of the first breakwater. Also, Fig. 13 shows the case of

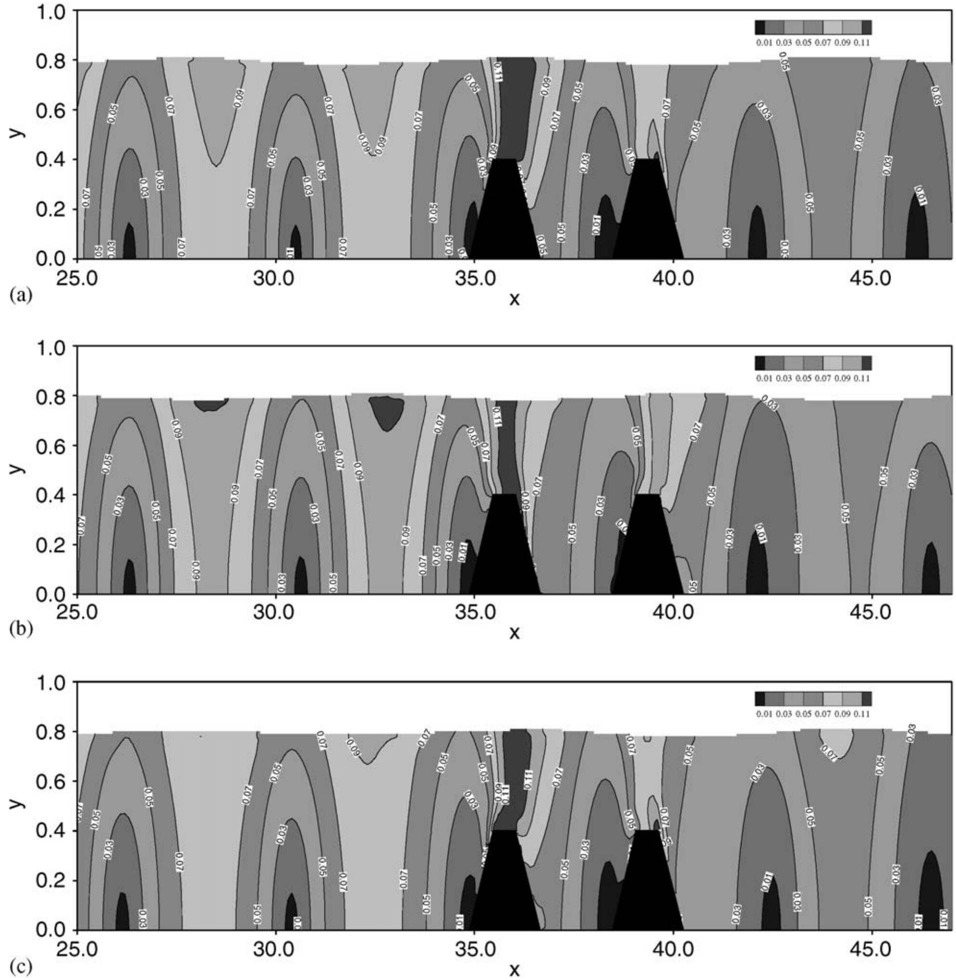

Fig. 10. Snapshots of velocity contour ($m = 2$).

submerged porous breakwaters of three arrays. As shown in Figs. 10–13, in all cases, the velocities become larger at the upper side of submerged breakwaters but decrease remarkably at the back side of the structures. This is caused by the fact that the energy of incident waves is considerably reflected by Bragg reflection effects due to submerged breakwaters.

7. Concluding remarks

In this study, numerical analyses and laboratory experiments are performed to investigate characteristics of the Bragg reflection due to multi-arrayed trapezoidal

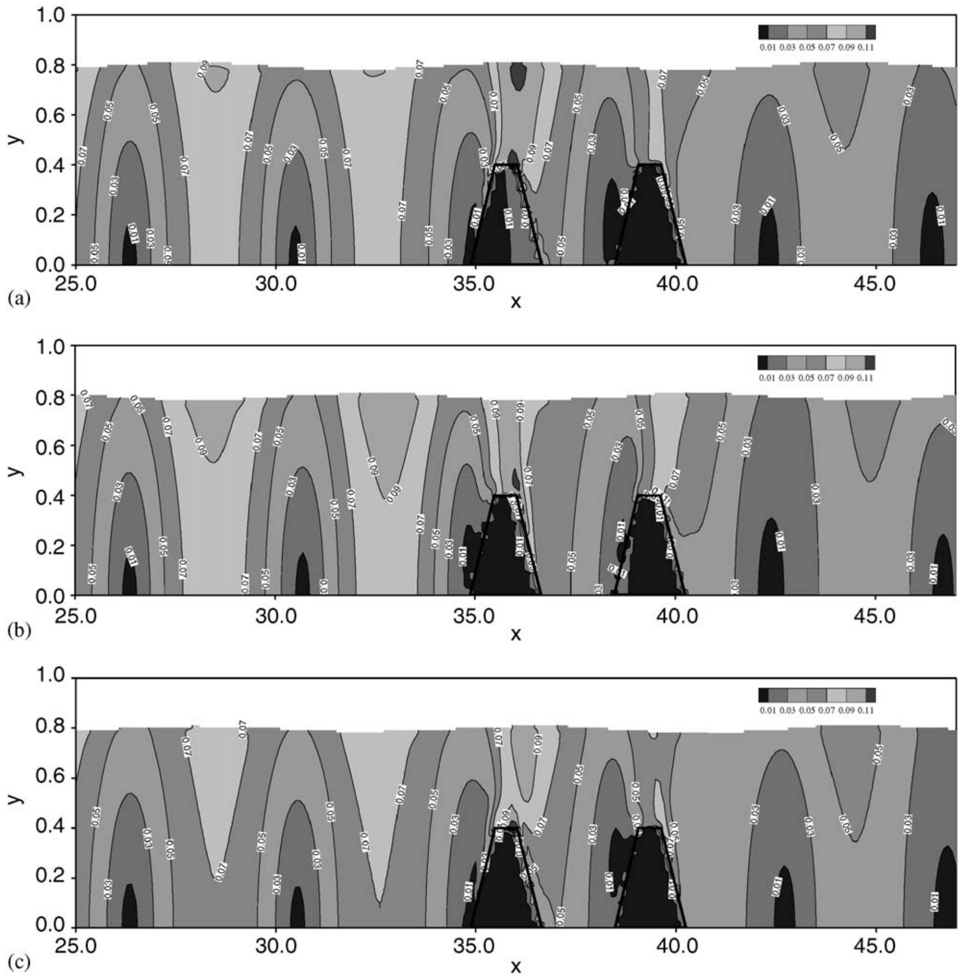

Fig. 11. Snapshots of velocity contour ($m = 2$, porous).

submerged breakwaters. The numerical model is based on the Reynolds averaged Navier–Stokes (RANS) equations with the VOF method and the k–ε turbulence closure model. In this model, it is possible to track the free surface displacements with accuracy and efficiency by the VOF method based on the density change equations.

The characteristics of the Bragg reflection for non-porous and porous break waters installed in one, two and three arrays are investigated in detail by numerical and laboratory experiments. And the results based on the EFEM model are also compared for non-porous structures. As a result of this study, it is noted that the reflection coefficients increase as the number of

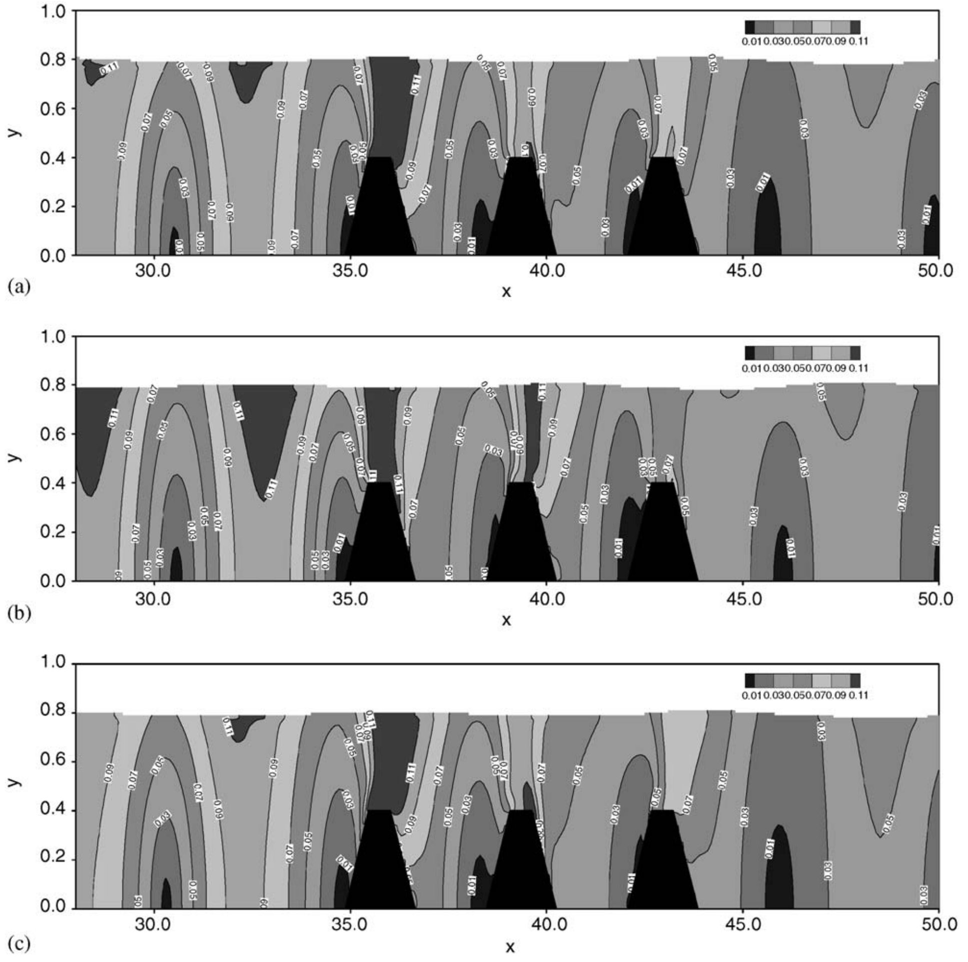

Fig. 12. Snapshots of velocity contour ($m = 3$).

submerged breakwaters increases, and the resonance period shows similar values of the relative wave number regardless of the permeability and the number of arrays. The reflection coefficients due to porous breakwaters are smaller than those due to non-porous breakwaters. For short waves, the effects of the permeability of the structures may be negligible on the magnitude of reflection.

Furthermore, the velocity contours in the case of two and three arrays are described. The velocities become larger at the upper side of submerged structures and decrease at the back side. This is caused by the fact that a significant amount of the incident wave energy is reflected by the Bragg reflection effects due to submerged breakwaters.

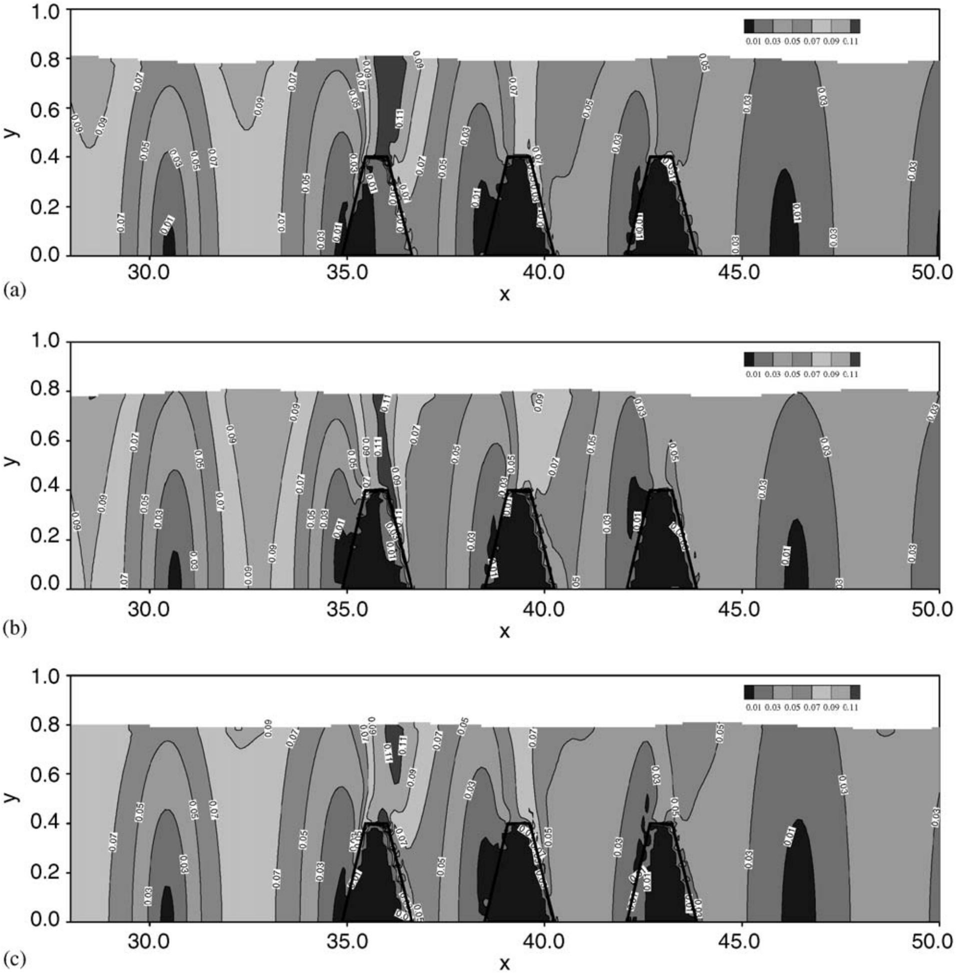

Fig. 13. Snapshots of velocity contour ($m = 3$, porous).

Acknowledgment

This research was financially supported by the Korea Sea Grant Program of the Ministry of the Maritime Affairs and Fisheries, Korea.

References

Cho, Y.-S., Yoon, S.B., Lee, J.-I., Yoon, T.-H., 2001. A concept of beach protection with submerged breakwaters. Journal of Coastal Research 34 (special issue), 671–678.

Cooker, M.J., Peregrine, D.H., Vidal, C., Dold, J.W., 1990. The interaction between a solitary wave and a submerged semicircular cylinder. Journal of Fluid Mechanics 215, 1–22.

Goda, Y., Suzuki, Y., 1976. Estimation of incident and reflected waves in random wave experiments. In: Proceedings of the 15th International Conference on Coastal Engineering, Hawaii, USA, pp. 828–845.

Hirt, C.W., Nichols, B.D., 1981. Volume of fluid (VOF) method for the dynamics of free boundaries. Journal of Computational Physics 39, 201–225.

Hwung, H.-H., Tu, S.-Y., Hwang, K.-S., 2002. The interaction of a solitary wave and a submerged porous breakwater. In Proceedings of the Fifth International Conference on Hydrodynamics, Tainan, 365–370.

Lin, P., 1998. Numerical modeling of breaking wave. Ph.D. Thesis, Cornell University, Ithaca, NY.

Lin, P., Liu, P.L.-F., 1998. A numerical study of breaking waves in the surf zone. Journal of Fluid Mechanics 359, 239–264.

Liu, P.L.-F., Lin, P., 1997. A numerical model for breaking wave: the volume of fluid method. Research Report CACR-97-02, Ocean Engineering Laboratory, Center for Applied Coastal Research, University of Delaware, Newark, Delaware.

Liu, P.L.-F., Lin, P., Chang, K.-A., Sakakiyama, T., 1999. Numerical modeling of wave interaction with porous structures. Journal of Waterway, Port, Coastal, and Ocean Engineering, ASCE 25 (6), 322–330.

Losada, I.J., Patterson, M.D., Losada, M.A., 1997. Harmonic generation past a submerged porous step. Coastal Engineering 31, 281–304.

Mase, H., Oki, K., Kitano, T., Mishima, T., 2000. Experiments on Bragg scattering of waves due to submerged breakwaters. In: Coastal Structures '99, pp. 659–665.